



City Research Online

City St George's, University of London

Citation: Morgan, M. J., Mareschal, I., Chubb, C. & Solomon, J. A. (2012). Perceived pattern regularity computed as a summary statistic: implications for camouflage. *Proceedings of the Royal Society B: Biological Sciences*, 279(1739), pp. 2754-2760. doi: 10.1098/rspb.2011.2645

This is the accepted version of the paper.

This version of the publication may differ from the final published version. To cite this item please consult the publisher's version.

Permanent repository link: <https://openaccess.city.ac.uk/id/eprint/14136/>

Link to published version: <https://doi.org/10.1098/rspb.2011.2645>

Copyright and Reuse: Copyright and Moral Rights remain with the author(s) and/or copyright holders. Copies of full items can be used for personal research or study, educational, or not-for-profit purposes without prior permission or charge, unless otherwise indicated, provided that the authors, title and full bibliographic details are credited, a hyperlink and/or URL is given for the original metadata page and the content is not changed in any way. For full details of reuse please refer to [City Research Online policy](#).

**PERCEIVED PATTERN REGULARITY COMPUTED AS A
SUMMARY STATISTIC: IMPLICATIONS FOR CAMOUFLAGE**

Journal:	<i>Proceedings B</i>
Manuscript ID:	RSPB-2011-2645.R1
Article Type:	Research
Date Submitted by the Author:	n/a
Complete List of Authors:	Morgan, Michael; Max-Planck Institute for Neurological Research, Visual Perception Solomon, Joshua; City university, optometry Chubb, Charles; UC Irvine, Mareschal, isabelle; City University, Optometry
Subject:	Behaviour < BIOLOGY, Biophysics < BIOLOGY, Computational biology < BIOLOGY
Keywords:	Vision, Texture, Camouflage
Proceedings B category:	Neuroscience

SCHOLARONE™
Manuscripts

1

2

3

4 PERCEIVED PATTERN REGULARITY
5 COMPUTED AS A SUMMARY STATISTIC:
6 IMPLICATIONS FOR CAMOUFLAGE

7

8

9

10 M.J. Morgan^{1,2}

11 I.^{2,4}

12 C. Chubb³

13 J.A. Solomon²

14

15 ¹ Max-Planck Neurology Institute, Koeln, Germany

16 ² Optometry Department, City University, London, UK

17 ³ University of California at Irvine, CA, USA

18 ⁴ School of Psychology. University of Sydney, 20006 NSW, Australia

19

20 Corresponding author:

21 Michael Morgan

22 Max-Planck-Institute for Neurological Research

23 50 Gleuler Strasse, Koeln, Germany

24 Michael.Morgan@nf.mpg.de

25

26 Abstract

27 Why do the equally spaced dots in Figure 1 appear regularly spaced? The
28 answer ‘because they are’ is naïve and ignores the existence of sensory
29 noise, which is known to limit the accuracy of positional localization
30 (Barlow, 1977; Levi & Klein, 1982; Levi & Klein, 1986; Morgan, 1990;
31 Morgan, Hole, & Ward, 1990; Watt & Hess, 1987; Westheimer, 1981).
32 Actually, all the dots in Figure 1 have been physically perturbed, but in
33 the case of the apparently regular patterns to an extent that is below
34 threshold for reliable detection. Only when retinal pathology causes
35 severe distortions do regular grids appear perturbed. Here we present
36 evidence that low-level sensory noise does indeed corrupt the encoding of
37 relative spatial position, and limits the accuracy with which observers can
38 detect real distortions. The noise is equivalent to a Gaussian random
39 variable with a standard deviation of ~5% of the inter-element spacing.
40 The just-noticeable difference in positional distortion between two
41 patterns is smallest when neither of them is perfectly regular. The
42 computation of variance is statistically inefficient, typically using only 5
43 or 6 of the available dots.

44

45

46 Introduction

47 The idea that perceptual systems are tuned to look for regularities and
48 structures in the environment was proposed by the Gestalt Psychologists
49 (Koffka, 1935), but we know little about the mechanisms for perceiving
50 regularities, or their limits. Patterns such as those in Fig. 1 are perceived
51 by normal observers as more-or-less regular, but we do not know what
52 mechanisms they use to decide whether the patterns are completely
53 regular or not. In particular, it is not clear how the observer treats sensory
54 noise in the representation of regularity. The existence of this noise can
55 be demonstrated using dots similar to the individual texture elements in

56 Fig. 1. When observers are shown 3 dots in a row and have to decide
57 whether the centre one is ‘up’ or ‘down’ relative to the position of the
58 flankers, they do not always give the same answer at a given physical
59 displacement of the centre dot. Sensory noise is responsible for this
60 variability (Green & Swets, 1966).

61 It is conventional to represent performance with a ‘Psychometric
62 function’ that relates response probabilities to the physical stimulus. An
63 example for the alignment of 3 dots is shown in Fig. 2. Good fits to
64 Psychometric functions for such alignment tasks are usually obtained by
65 assuming the sensory noise is Gaussian, with a standard deviation equal
66 to a size difference of ~5% (Westheimer, 1981; Morgan, 1990)

67 If this sensory noise were included in the perceptual representation of a
68 pattern with regularly-spaced elements, we would expect to see local
69 irregularities throughout the pattern, even when none are physically
70 present. The alignments between elements would all seem different.
71 Some of the differences, by chance, would be larger than the standard
72 deviation of the noise, and should thus be conspicuous. However, this is
73 not what happens. Instead, a regular pattern appears regular. We now
74 consider two alternative hypotheses to account for this finding.

75 (1) The Undersampling Model. Observers are unable to measure the
76 spatial relationships between all the elements during a brief
77 glimpse of the pattern. Instead, they take a restricted sample of
78 elements, and use only these elements to calculate the positional
79 variance. They can use the computed variance to decide whether
80 one pattern is more regular than another. However, the variance
81 is only represented in perception if it exceeds the amount
82 expected from sensory noise. Thus all patterns with physical
83 variances smaller than the sensory noise will appear completely
84 regular, even if they can be discriminated. It may seem
85 paradoxical that an observer could discriminate differences in
86 patterns that ‘look’ the same but there are many examples of this
87 in the ‘discrimination without awareness’ literature (He,

88 Cavanagh, & Intriligator, 1996; Parkes, Lund, Angelluci,
89 Solomon, & Morgan, 2001; Smallman, MacLeod, He, &
90 Kentridge, 1996.) The key to this dissociation is that in the
91 discrimination case the observer is forced to decide which of two
92 patterns is more regular: a decision they can make without
93 adapting any absolute standard of complete regularity. In the
94 ‘appearance’ case they have to decide whether a given pattern is
95 completely regular or not. To make this decision they have to
96 adopt some criterion, and this may well depend upon their own
97 sensory noise.

98 (2) The Sensory Threshold model. The observer calculates a variance
99 signal from all or some of the pattern elements, but all variances
100 falling below some arbitrary “sensory threshold” are set to zero.
101 This is *not* the same as the threshold implicit in the
102 Undersampling model because the threshold in the latter case
103 does not affect the discrimination process, only the conscious
104 decision whether a pattern is, or is not, regular.

105 To decide between these two models on a quantitative basis we
106 measured the ability of observers to discriminate between pairs of
107 patterns such as those in Figure 1 when they were both irregular, but
108 to different extents. One of the patterns had a variance σ^2 and the
109 other a variance $\sigma^2 + \Delta\sigma^2$. A key prediction of the Sensory Threshold
110 Model is that the best performance (the lowest $\Delta\sigma^2$) will be obtained
111 when V is non-zero. In other words, two patterns will be more easily
112 discriminated when both are slightly irregular than when one of
113 them is completely regular. Exactly this effect, referred to as
114 ‘pedestal facilitation’ has been reported for the discrimination of
115 luminance contrast, and has been conventionally explained by a
116 sensory threshold (Nachmias & Sansbury, 1974 ; for recent review
117 see Solomon, 2009). The Undersampling model does not predict
118 pedestal facilitation of variance, although as we shall see, this depends on
119 the exact measure we take of the threshold. The final decision between

120 the two models can only be taken by their goodness-of-fit to the data,
121 which we assess using the calculation of maximum likelihood.

122 A second question we addressed in these experiments is how the presence
123 of task-irrelevant variance in the patterns would affect variance
124 discrimination along the relevant dimension. In all cases, the relevant
125 dimension was the positional variance of the dots. In one manipulation
126 we added irrelevant variance of contrast between the elements comprising
127 the patterns. In another manipulation we arranged the dots around a
128 circle and instructed observers to report the variance in either their
129 angular separation or their distance from the centre, ignoring the other
130 dimension. These investigations bear on the general theory of
131 camouflage. Previous psychophysical investigations of camouflage have
132 used variance in an irrelevant dimension to mask a pattern defined by its
133 *mean* difference from the background (e.g. Callaghan, 1984). Here we see
134 if this generalizes to the masking of *variance* by variance.

135 Methods

136 *Observers.* The observers were two of the authors (MM and IM) and a
137 third (GM) who was unaware of the specific aims of the experiment.

138 *Apparatus.* Stimuli were presented on the LCD screen of a Sony Vaio
139 (PGC-TR5MP) laptop computer using MATLAB and the PsychToolbox
140 (Brainard, 1997) for Windows. Screen size was 1280 x 768 pixels (230 x
141 14 mm). Only the Green LCD's were used, and the mean luminance was
142 56 cd/m². The viewing distance was approximately 57 cm so that the
143 pixel size was approximately 0.018 deg of visual angle.

144 *Stimuli.* Different kinds of regular patterns were used in different
145 experiments. In square arrays the dots were regularly spaced in an 11 x
146 11 lattice (Figure 1). In circular patterns 11 dots were equally spaced
147 around a notional circle. In linear patterns 11 dots were equally spaced
148 along a notional line. The position of each dot in the array was selected
149 from a uniform probability density function with mean μ and range ω ,
150 where μ was the position it would have if the pattern were completely

151 regular. In the square arrays the spatial perturbation was independently
152 sampled in dimensions x and y . In the circular patterns the perturbation
153 was either radial or angular in different experiments. We also included
154 ‘camouflage’ conditions where (a) observers had to ignore irrelevant
155 variation to the radial position of the dots while responding to variation in
156 their angle, and (b) observers ignored random contrast polarity (black vs.
157 white) of the dots in the circular array, while responding to variance in
158 angular position. All dots had a Gaussian profile with a space constant of
159 one quarter of the inter-dot separation, making them look slightly fuzzy.

160 *Procedure.* On each trial two patterns were shown, each for 200 msec and
161 with a 200-msec blank interval in between. Observers had to decide
162 which of the two had the greater degree of spatial irregularity. The
163 reference pattern with pedestal range ω was presented randomly either
164 first or second. The standard deviation of the range is related to its width
165 ω by the expression $\sigma = \omega / \sqrt{12}$. The position of each dot in the other
166 pattern, the test, had a range of $\omega + \Delta\omega$, where $\Delta\omega$ was varied by an
167 adaptive procedure (QUEST, Watson & Pelli, 1983) to determine the
168 just-noticeable $\Delta\omega$ (JND) at which the observer was 82% correct. There
169 was no feedback to indicate whether the response was correct or not. The
170 pedestal range was randomly selected on each trial from a set of preset
171 values. A block of trials terminated when each of these preset values had
172 been presented 50 times. Confidence limits for the JND (95%) were
173 determined by exactly simulating the experiment 80 times with a
174 bootstrapping procedure (Efron, 1982).

175 *Modeling.* The model assumes that the observer samples elements (dots)
176 from the grid and compares their positions to those predicted from a
177 template. We admit that this version of the model is unrealistic. It is
178 more likely that the observer has access to sensory signals representing
179 the alignment between pairs of dots (Fig. 2) or their separations.
180 However, such a model is difficult to compute, particularly in the two
181 dimensions of a grid. The model we actually use should be thought of as

182 an ideal observer model in which the observer knows the positions of all
183 the dots in a template.

184 In the Undersampling model, the observer on each trial samples v dot
185 positions from each of the two patterns and selects the pattern having the
186 greater sample variance of these positions from the template positions. In
187 the case of the standard pattern, each of the the v dots is taken from a
188 distribution with variance $\omega^2/12 + \tau^2$, where τ is the standard deviation of
189 the internal noise, and in the case of the test pattern each is taken from a
190 distribution with variance $(\omega + \Delta\omega)^2/12 + \tau^2$. Recall that the external
191 perturbations were taken from a uniform distribution of width ω which
192 has variance $\omega^2/12$). The units of ω are the distance between elements in
193 the unperturbed pattern. When the underlying probability density
194 functions (pdf) for signal, pedestal and noise are Gaussian it is easy to
195 compute the probability that $\text{var}(\text{test})/\text{var}(\text{ref}) > 1$ and thus that the
196 observer is correct (Morgan, Chubb, & Solomon, 2008). However,
197 departures from regularity in our stimuli did not form Gaussian
198 distributions, so we resorted to simulation to produce the fits shown in
199 Figure 2. The fits had only two free parameters, the number of dots per
200 sample (v) and the range of the internal noise in the same units as ω . The
201 Sensory Threshold model was the same as the Undersampling model,
202 except that all internal variances below a threshold value were set to zero
203 before the two stimuli were compared. This latter model has three
204 parameters, the internal noise, the number of dots per sample, and the
205 threshold.

206 *Significance testing.* The experimental data for each condition consisted
207 of a $3 \times N$ matrix, where N was the number of trials in the condition to be
208 analysed. The first row of the matrix contained the pedestal value ω , the
209 second the value of $\Delta\omega$ and the third the observer's response (0 for
210 wrong, and 1 for correct). The model used the values of ω and $\Delta\omega$ along
211 with the estimated values for the number of dots per sample and the
212 internal noise to predict the probability correct, which was then compared

213 to the actual observer's responses to calculate the joint likelihood over all
214 N trials

215 The Matlab function *fminsearch* was the used to find values of internal
216 noise (τ) and sample size (ν) to maximize the joint likelihood. In
217 practice, to avoid non-integral values of ν , we used fixed values of
218 sample size to find the best fitting internal noise, and repeated this
219 procedure over a range of sample sizes to find the best overall fit.

220 The calculation of probability correct for a particular combination of
221 $\{\nu, \tau, \omega, \Delta\omega\}$ was calculated from 10,000 simulated trials. To make
222 possible an orderly gradient descent we seeded the random number
223 generator used by the simulator so that each combination of
224 $\{\nu, \tau, \omega, \Delta\omega\}$ always produced exactly the same probability correct. To test
225 the reliability of the fits we carried out 80 independent fits with different
226 seeds for the random number generator, and used the resulting
227 distribution of fits to calculate 95% confidence limits. These were always
228 well within the confidence limits of the thresholds estimated from the
229 data by bootstrapping.

230

231 **Results**

232 **(A) Discrimination Thresholds as function of Pedestal**

233 We present first (Fig. 3) the results for one subject (MM) in one condition
234 (11 x 11 grid) in order to establish some general points about the data and
235 modeling. The figure shows, on the left, the JND's in the standard
236 deviation of the added noise, as a function of the standard deviation of the
237 pedestal. Recall that the pedestal refers to the noise in the less variable
238 stimulus, while the discrimination threshold is how much more noise the
239 other stimulus needs for the two to be discriminable at the 84% correct
240 level. An important point to note is that the models are constrained not
241 just by the points shown in this graph, but by all the points on the
242 psychometric function (Fig. 1) amounting to several thousands of trials.

243 The data points show a clear ‘dipper’ effect with a minimum threshold
244 (best discrimination) at a non-zero value of the pedestal. Thereafter they
245 show an increase as a function of pedestal level, approximating a slope of
246 unity. This effect is conventionally called ‘masking’ of the added signal
247 by the pedestal and is related to Weber’s Law, which states that the JND
248 between two stimuli is proportional to their absolute magnitude (review
249 by Solomon, 2009 ; Laming, 1985).

250 The best fit to the data is the solid curve running through all the data
251 points. This is the fit of the Undersampling Model, which contains two
252 parameters, the internal noise of the observer and the number of dots per
253 sample used by the observer to calculate the variance (in this case, 6 out
254 of the 11 x 11 available). Note that this model does *not* include a sensory
255 threshold. It may seem puzzling, therefore, that it produces a ‘dip’, which
256 is conventionally explained by a sensory threshold. The reason for this is
257 shown in the graph on the right, which plots the same data in terms of the
258 *variance* of the noise and the pedestal, rather than its standard deviation.
259 The ‘dip’ now disappears, both from the data and from the model. The
260 reason for the ‘dip’ in the standard deviations (left hand figure) is that in
261 the model the internal noise of the observer and the external noise added
262 to the stimulus are assumed to be additive. In a linear system two
263 independent noise sources are equivalent to a single noise having the sum
264 of the two variances. This squaring means that the larger of the two noise
265 sources is dominant. When the two stimuli being compared have no
266 external noise the internal noise predominates and the observer is
267 relatively insensitive. When both stimuli have a pedestal equal to the
268 internal noise the latter is less dominant and discrimination is easier. For
269 example, let the internal noise have unit standard deviation, let the
270 pedestal be zero, and let the other stimulus have a standard deviation that
271 is one more than the pedestal. The difference in standard deviation
272 between the two stimuli is $\sqrt{1^2 + (0 + 1)^2} - \sqrt{1^2 + 0^2} = .4142$.
273 Now let the pedestal also have unit standard deviation. The same
274 calculation produces the difference $\sqrt{1^2 + (1 + 1)^2} - \sqrt{1^2 + 1^2} =$

275 .8219. Therefore, the effect of the signal is greater with a non-zero
276 pedestal.

277 The apparent ‘dip’ disappears when variances are plotted instead. The
278 ‘dip’ on the left-hand side of Fig. 3 is therefore *not* evidence for a sensory
279 threshold. To see what the effect of a sensory threshold would actually
280 be, we plot the case where there is a sensory threshold equal to the
281 variance of internal noise. This produces the steeply-dipped function in
282 Fig. 1 (left). It also produces a dip in the variance plot (right).

283 Note that the Undersampling model also predicts the ‘masking’ region of
284 the dipper function, where thresholds rise with the pedestal value. This is
285 particularly clear in the variance plot (right hand figure). The reason for
286 this is that the sampling variance of the variance rises with the true
287 variance. On each trial the observer is comparing two sample variances.
288 The greater the true variance (the pedestal) the more likely the two
289 samples are to differ by chance, and the larger the signal will have to be
290 in order to be reliably detected. All this is as predicted by the model.

291 Figure 3 also plots functions when the number of samples is equal to the
292 total number available (11 x 11) or equal to only 2. These are
293 significantly poor fits to the data, as verified by a bootstrapping test based
294 on likelihoods.

295

296 The model fits to the data for all conditions (e.g. 11 dots in a circle;
297 Single row of 11 dots) are shown in Table 1, and illustrative examples are
298 shown in Fig. 4. The Table shows that observers always used fewer than
299 the number of dots available, typically ~6, and that the Sensory Threshold
300 model was never a significantly better fit to the data than the simple
301 Undersampling Model. In no case was the fitted threshold as high or
302 higher than the fitted internal noise.

303 **(B) Camouflage**

304 We collected two kinds of data relevant to camouflage. In the first, a
305 circular array of dots was used and the elements were perturbed in their
306 angle from the centre. Either all had the same contrast, or were randomly
307 black or white. The observers were MM, GM and IM. As Table 1 and
308 Fig. 4 show, the contrast variation caused an increase in thresholds, even
309 though it was irrelevant to the task. The effect on the model fits was that
310 contrast variation was equivalent to an increase in sensory noise. This is
311 also true of the second test, where a radial variation in dot position was
312 camouflaged by an irrelevant perturbation in the angle (observers MM
313 and GM), except that there was a decrease in the number of samples from
314 5 to 4 for MM in the camouflage condition.

315 **Discussion**

316 We suggest two related conclusions. The first is that the observer's
317 discrimination performance is limited by low-level noise equivalent to
318 physical perturbation in the position of the dots. This means that a
319 completely regular pattern is not discriminable from one having a marked
320 degree of physical perturbation. However, both such patterns appear
321 completely regular (Figure 1). The low-level noise is not represented in
322 awareness. We infer from this that the internal noise in individual dot
323 position is *not* represented in the conscious perception of a regular
324 pattern. Rather, what is represented is a regular template for the pattern. If
325 the computed perturbation from the template does not exceed the internal
326 noise level, then the pattern is seen as regular.

327 This conclusion is reinforced by our estimates of the number of dots
328 (v) the observer is using in computing variability. We estimate this
329 number as ~ 6 , which is strikingly inefficient for a pattern with 11 x 11
330 elements. The efficiency is higher ($\sim 50\%$) for the circular patterns but v
331 is still ~ 6 , suggesting a fixed sample size rather than a fixed efficiency.
332 The only exception to the ' $v=6$ ' rule is observer IM who manages an
333 impressive 11 dots for the 11 x 11 pattern. The conclusion that observers
334 use only a small amount of the available information to compute
335 irregularity is further evidence that the perception of a regular pattern is

336 the perception of a template, since the actual physical position of most of
337 the dots are not being represented at all. In other words, we see a regular
338 arrangement of dots, even though the noisy position of many of them has
339 not been sampled.

340 Our findings also suggest a general theory of pattern camouflage. In its
341 most general form the principle of camouflage is that irrelevant variation
342 along one dimension masks detection of variation along another. For
343 example, a region of high orientation variance if a texture is harder to see
344 in the texture elements are randomly coloured red and green (Callaghan,
345 1984; Morgan, Adam, & Mollon, 1992). This is analogous to what we
346 find in our experiments for variance. The ability of observers to detect
347 perturbations of radial position in circular patterns is compromised by
348 irrelevant contrast variation or by angular variation. This is what we
349 would expect if observers were computing variance from a fixed internal
350 template.

351 Acknowledgments. We thank the UK EPSRC Research Council (grant
352 EP/H033955/1) and the Max-Planck Society for support.

353

354

355

356

357

358

359

360

361

362

363 Table

Condition	ι	Thresh	ν	Log Likelihood	ChiSq
1 MM Circ Rad 1	0.07		5	-940.10	
2 MM Circ Rad 2	0.07	0.02	5	-940.15	
3 MM Circ Rad Rand Ang 1	0.09		4	-833.71	
4 MM Circ Rad Rand Ang 2	0.09	0.01		-833.00	
5 MM 1 and 3 combined	0.07		4	-1785.60	-23.58
6 GM Circ Rad 1	0.06		4	-699.59	
7 GM Circ Rad 2	0.06	0.00	5	-699.20	
8 GM Circ Rad Rand Ang 1	0.09		4	-821.34	
9 GM Circ Rad Rand Ang 2	0.09	0.06	6	-821.27	
10 GM 6 and 8 combined	0.08		4	-1534.80	-27.74
11 MM Circ Ang 1	0.11		5	-1371.30	
12 MM Circ Ang 2	0.20	0.38	5	-1371.30	
13 MM Circ Ang Rand B/W 1	0.15		5	-1895.40	
14 MM Circ Ang Rand B/W 2	0.15	0.12	5	-1895.30	
15 MM 11 and 13 combined	0.13		5	-3350.70	-168.00
16 IM Circ Ang 1	0.11		5	-661.30	
17 IM Circ Ang 2	0.11	0.08	5	-661.28	
18 IM Circ Ang Rand B/W 1	0.13		5	-703.17	
19 IM Circ Ang Rand B/W 2	0.13	0.05	6	-703.17	
20 IM 16 and 18 combined	0.12		6	-1370.70	-12.46
21 GM Circ Ang 1	0.11		6	-753.02	
22 GM Circ Ang 2	0.11	0.08	6	-753.02	
23 GM Circ Ang Rand B/W 1	0.12		5	-792.96	
24 GM Circ Ang Rand B/W 2	0.12	0.11	5	-792.84	
25 GM 21 and 23 combined	0.11		5	-1550.30	-8.64
26 MM 11 x 11 1	0.08		6	-1321.80	
27 MM 11 x 11 2	0.13	0.07	6	-736.40	
28 IM 11 x 11 1	0.13		11	-736.41	
29 IM 11 x 11 2	0.13	0.11	11	-736.37	
30 MM 1 x 11 1	0.07		5	-671.97	
31 MM 1 x 11 2	0.07	0.00	5	-671.96	
32 IM 1 x 11 1	0.07		5	1327.10	
33 IM 1 x 11 2	0.07	0.00	5	1327.10	

364

365 The Table shows best-fitting values for internal noise, sample size
 366 (ν) and threshold (t) to the data for different observers and
 367 conditions (key in second column) along with the log likelihoods of
 368 these fits (column 6). The unit for ι is the proportion of nearest-
 369 neighbour spacings in each array. The final column (χ^2) shows the
 370 values for twice the difference in log likelihoods of two fits. Fits with
 371 a threshold such as Row 2 are compared to fits without in the row
 372 above. Fits that combine two conditions, such as Row 5, which
 373 combines 1 and 3, are compared to the summed likelihoods of the
 374 two separate fits.

375

376

377

378 REFERENCES

379

- 380 Barlow, H. B. (1977). Retinal and central factors in human vision
 381 limited by noise. In H. B. Barlow & P. Fatt (Eds.), *Vertebrate*
 382 *Photoreception*. New York: Academic Press.
- 383 Brainard, D. H. (1997). The Psychophysics Toolbox. *Spat Vis*, 10, 433-
 384 436.
- 385 Callaghan, T. (1984). . Dimensional interaction of hue and brightness
 386 in preattentive field segregation. *Perception & Psychophysics* .
 387 36, 25--34.
- 388 Efron, B. (1982). *The Jackknife, the Bootstrap and Other Resampling*
 389 *Plans*. Philadelphia: Society for Industrial and Applied
 390 Mathematics.
- 391 Green, D. M., & Swets, J. A. (1966). *Signal Detection Theory and*
 392 *Psychophysics* (1 ed.). New York: Wiley.
- 393 He, S., Cavanagh, P., & Intriligator, J. (1996). Attentional resolution
 394 and the locus of visual awareness. *Nature*, 383, 334-337.
- 395 Koffka, K. (1935). *Principles of Gestalt Psychology*. London: Lund
 396 Humphries.
- 397 Laming, D. (1985). Some principles of sensory analysis. *Psychological*
 398 *review*, 92(4), 462-485.
- 399 Levi, D. M., & Klein, S. A. (1982). Hyperacuity and amblyopia. *Nature*,
 400 298, 268-270.
- 401 Levi, D. M., & Klein, S. A. (1986). Sampling in spatial vision. *Nature*,
 402 320(27 March), 360-362.
- 403 Morgan, M., Chubb, C., & Solomon, J. A. (2008). A 'dipper' function for
 404 texture discrimination based on orientation variance.
 405 [Research Support, Non-U.S. Gov't]. *Journal of Vision*, 8(11), 9
 406 1-8. doi: 10.1167/8.11.9
- 407 Morgan, M. J. (Ed.). (1990). *Hyperacuity*. London: Macmillan.
- 408 Morgan, M. J., Adam, A., & Mollon, J. D. (1992). Dichromats break
 409 colour-camouflage of textural boundaries. *Proc. Roy. Soc., B*.
 410 248, 291-295.
- 411 Morgan, M. J., Hole, G. J., & Ward, R. M. (1990). Evidence for positional
 412 coding in hyperacuity. *J.opt.Soc.Am. A*, 7, 297-304.
- 413 Nachmias, J., & Sansbury, R. (1974). Grating contrast: discrimination
 414 may be better than detection. *Vision Research*, 14 1039-1042
- 415 Parkes, L., Lund, J., Angelluci, A., Solomon, J., & Morgan, M. (2001).
 416 Compulsory averaging of crowded orientation signals in
 417 human vision. *Nature Neuroscience*, 4, 739-744.
- 418 Smallman, H. S., MacLeod, D. I. A., He, S., & Kentridge, R. W. (1996).
 419 Fine-grain of the neural representation of human spatial
 420 vision. *J. Neurosci.*, 16, 1852-1859.

- 421 Solomon, J. A. (2009). The history of dipper functions. [Historical
422 ArticleReview]. *Attention, perception & psychophysics*, 71(3),
423 435-443. doi: 10.3758/APP.71.3.435
- 424 Watson, A. B., & Pelli, D. G. (1983). QUEST: A Bayesian adaptive
425 psychometric method. *Perception and Psychophysics*, 33(2),
426 113-120.
- 427 Watt, R. J., & Hess, R. F. (1987). Spatial information and uncertainty in
428 anisometric amblyopia. *Vision Research*, 27, 661-674.
- 429 Westheimer, G. (1981). Visual Hyperacuity. *Progress in Sensory*
430 *Physiology* 1, 2-29.
- 431

For Review Only

432

433 Figure Legends

434 Fig. 1 legend. All 3 patterns contain 11 x 11 dots spaced on a regular grid
435 with individual dot positions independently perturbed by addition of a
436 random positional shift. In the leftmost pattern the random perturbation
437 is so small as to be invisible. In the middle pattern it is twice as great and
438 just visible. In the right-hand panel it is twice that of the middle panel and
439 is clearly visible.

440

441 Fig. 2 legend. The figure shows an example of a psychometric function
442 for discrimination with the best-fitting cumulative Gaussian fit (solid
443 curve) to the data points. The observer decided whether the centre dot in
444 a row of three dots was displaced 'up' or 'down' relative to the flanking
445 dots. Each data point shows the probability of responding 'up' (ordinate)
446 as a function of the actual physical displacement (abscissa). The vertical
447 bars represent 95% confidence limits from the binomial distribution.

448 Fig. 3 legend: The figure shows the results (filled circles) for observer
449 MM in the 11 x 11 grid condition, and the fits of various models
450 described more fully in the text. The panel on the left plots the data as a
451 function of the standard deviation of the uniform distribution from which
452 the dot positions were sampled, in units of the canonical dot spacing. The
453 panel on the right plots threshold $\Delta(\sigma^2)$ as a function of σ^2 . The red curve
454 passing through all the data points is the best fit of the Undersampling
455 model, with 6 dots per sample. The green curve is a fit of the Sensory
456 Threshold model with the threshold constrained to be the same as the
457 variance of the internal noise. The blue curve with the sharp dip in the
458 centre is the best fit of the Undersampling model with the number of
459 samples constrained to be the total number of dots (11 x 11). The black
460 curve with no 'dip' is the fit of the Undersampling model with $v=2$. In
461 the right hand panel only the best fits of the Undersampling model and
462 the Sensory Threshold model are plotted.

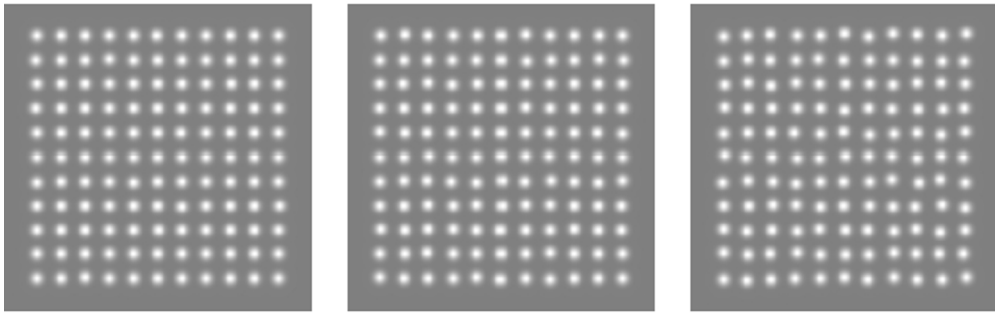
463

464 Fig. 4 legend. The top 4 panels (Fig 4a) show results for two observers
465 (MM left and IM right) with two kinds of stimulus array: 11 x 11 dot
466 matrices (top) and a single line of 11 dots (bottom). The solid line is the
467 best fit of the sampling model. The bottom four panels (Fig 4b) show
468 results for two observers (MM left, GM right) with arrays of 11 dots
469 arranged in a circle. In the top two panels the signal the observer was
470 instructed to compare between the two patterns in the 2AFC design was
471 the difference in variance of the radial distance of the dots. In the bottom
472 two panels, observers detected differences in angular separation of the
473 dots. In the condition indicated by square symbols, only the relevant
474 dimension was varied. In the condition indicated by circles, an additional
475 source of variation (camouflage) was introduced. In the top two panels
476 this was variation in angular position; in the bottom two panels it was
477 random variation in contrast polarity (white/black).

478

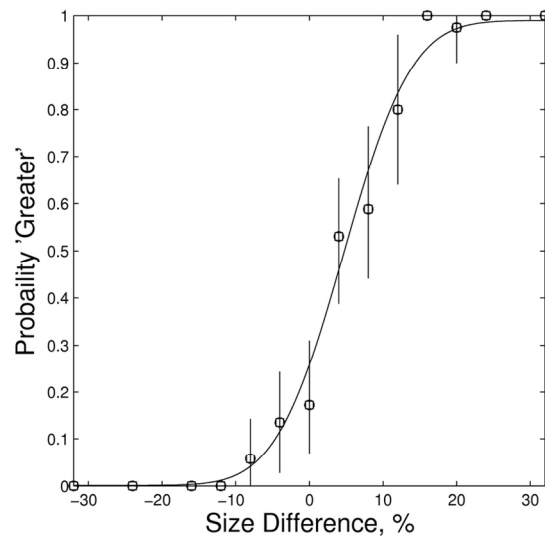
479

480



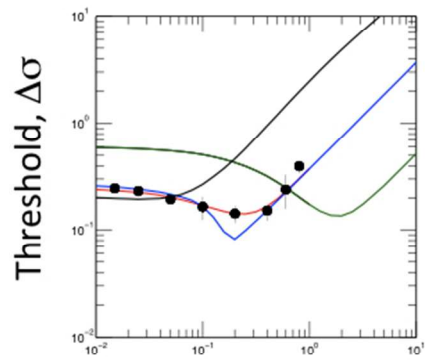
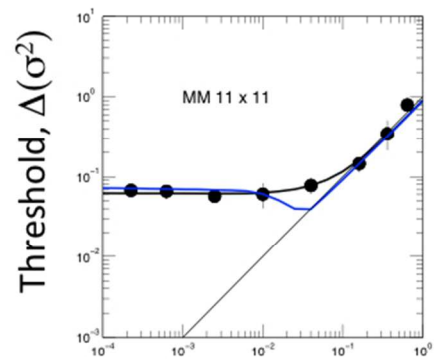
316x108mm (72 x 72 DPI)

For Review Only

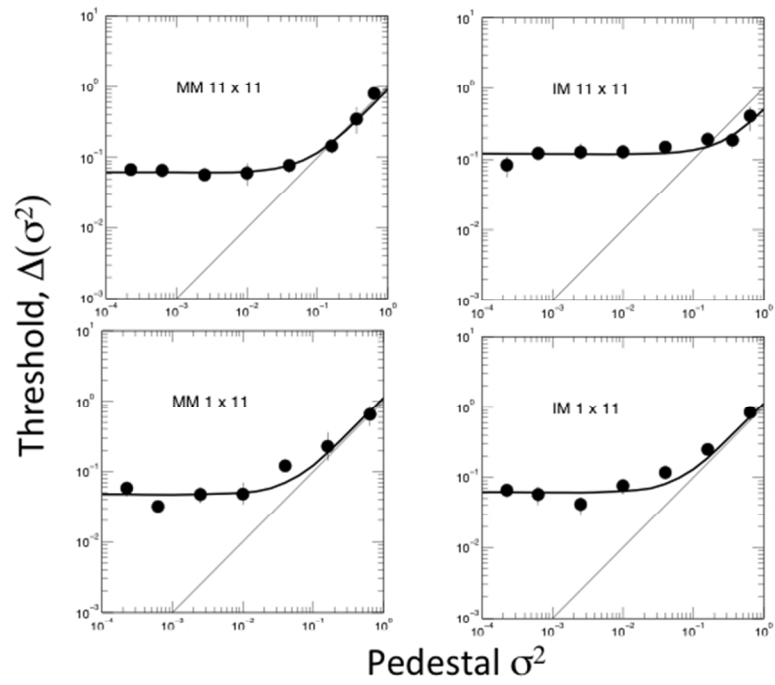


128x74mm (300 x 300 DPI)

View Only

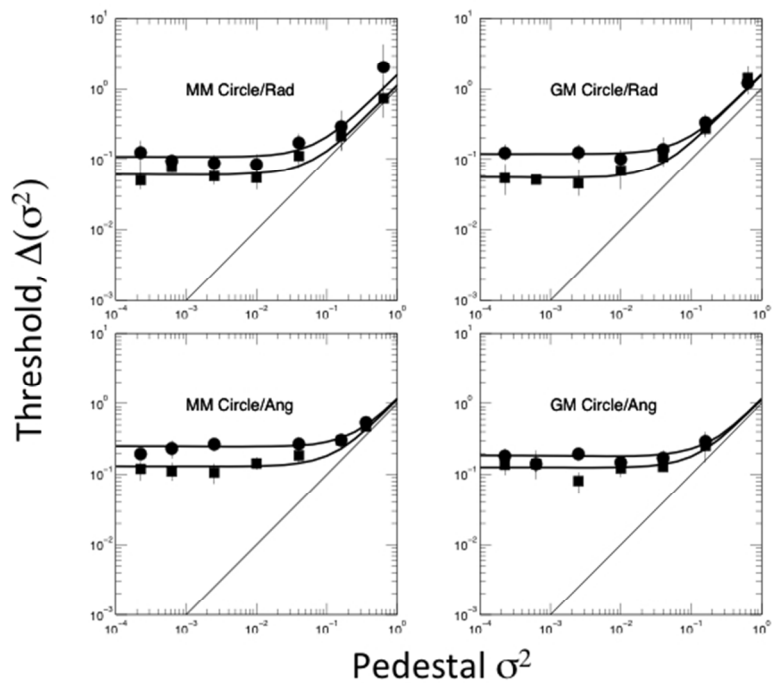
Pedestal σ Pedestal σ^2

254x190mm (72 x 72 DPI)



254x190mm (72 x 72 DPI)

View Only



254x190mm (72 x 72 DPI)